Check for updates

Stable potassium isotopes (^{41}K/^{39}K) track transcellular and paracellular potassium transport in biological systems

John A. Higgins[1]*, Danielle Santiago Ramos[2], Stefania Gili[1], Cornelia Spetea[3,4], Scott Kanoski[5], Darren Ha[6], Alicia A. McDonough[6] and Jang H. Youn[6]

[1]Department of Geosciences, Princeton University, Princeton, NJ, United States, [2]Department of Marine and Coastal Science, Rutgers University, New Brunswick, NJ, United States, [3]Department of Biological and Environmental Sciences, University of Gothenburg, Gothenburg, Sweden, [4]Department of Molecular Biology, Princeton University, Princeton, NJ, United States, [5]Department of Human and Evolutionary Biology, University of Southern California, Los Angeles, CA, United States, [6]Department of Physiology and Neuroscience, University of Southern California Keck School of Medicine, Los Angeles, CA, United States

As the most abundant cation in archaeal, bacterial, and eukaryotic cells, potassium (K^+) is an essential element for life. While much is known about the machinery of transcellular and paracellular K transport—channels, pumps, co-transporters, and tight-junction proteins—many quantitative aspects of K homeostasis in biological systems remain poorly constrained. Here we present measurements of the stable isotope ratios of potassium (^{41}K/^{39}K) in three biological systems (algae, fish, and mammals). When considered in the context of our current understanding of plausible mechanisms of K isotope fractionation and K^+ transport in these biological systems, our results provide evidence that the fractionation of K isotopes depends on transport pathway and transmembrane transport machinery. Specifically, we find that passive transport of K^+ down its electrochemical potential through channels and pores in tight-junctions at favors ^{39}K, a result which we attribute to a kinetic isotope effect associated with dehydration and/or size selectivity at the channel/pore entrance. In contrast, we find that transport of K^+ against its electrochemical gradient *via* pumps and co-transporters is associated with less/no isotopic fractionation, a result that we attribute to small equilibrium isotope effects that are expressed in pumps/co-transporters due to their slower turnover rate and the relatively long residence time of K^+ in the ion pocket. These results indicate that stable K isotopes may be able to provide quantitative constraints on transporter-specific K^+ fluxes (e.g., the fraction of K efflux from a tissue by channels vs. co-transporters) and how these fluxes change in different physiological states. In addition, precise determination of K isotope effects associated with K^+ transport *via* channels, pumps, and co-transporters may provide unique constraints on the mechanisms of K transport that could be tested with steered molecular dynamic simulations.

KEYWORDS

potassium, homeostasis, stable isotope, physiology, potassium channel, Na-K ATPase

1 Introduction

Archaeal, bacterial, and eukaryotic cells all concentrate potassium (K^+). In fact, the ubiquity of elevated intracellular K^+ has been hypothesized to provide insight into the environments (high K/Na ratios) where the first cells emerged (Mulkidjanian et al., 2012). In bacteria, intracellular K^+ is at >100 mM by the active pumping of K^+ from extracellular fluid (ECF) into the intracellular fluid (ICF) by transporters that use ATP or the proton motive force (Stautz et al., 2021). In eukaryotic cells, intracellular K^+ is maintained at similarly elevated levels by the active pumping of K^+ by plasma membrane Na,K-ATPase, an energetically intensive process which can account for ~20% of basal metabolism in mammals (Rolfe and Brown, 1997). In all cells, the active transport of K^+ into the cell establishes a steep transmembrane gradient that is a key determinant of membrane potential and a source of energy to drive action potentials, control muscle contractility, maintain cell turgor, contribute to pH homeostasis, and power ion transporters (Youn and McDonough, 2009; Stautz et al., 2021).

The regulation of K^+ at both the cellular and organismal level, K^+ homeostasis, is ultimately accomplished at the molecular level by transcellular and paracellular transporters (including ion pumps, channels, co-transporters) that move K^+ across membranes and between cells (Agarwal et al., 1994; Gierth and Mäser, 2007; Youn and McDonough, 2009; Furukawa et al., 2012). Although life has evolved a diversity of molecular machines capable of K^+ transport across cell membranes, certain aspects of cellular K^+ transport are conserved across the major domains. For example, all known K^+ channels are members of a single protein family whose amino acid sequence contains a highly conserved segment [the K^+ channel signature sequence (MacKinnon, 2003)]. The shared molecular machinery of K^+ transport in biological systems reflects the fundamental role of the electrochemical potential generated by biologically maintained gradients of K^+ across cell membranes. K^+ pumps establish and maintain concentration gradients across cell membranes by moving K^+ (from ECF-ICF) and Na or H (from ICF to ECF) "uphill" against their electrochemical potentials coupled to and driven by the hydrolysis of ATP. K^+ co-transporters couple uphill K^+ transport to "downhill" transport of another ion (e.g., Na^+ or Cl^-). Finally, K^+ channels and the pores in tight-junction proteins provide an energetically favorable pathway for rapid, yet highly selective, transport of K^+ down its electrochemical potential.

While the identity and structure of the molecular machines that maintain K^+ homeostasis in biological systems are well-known, many quantitative aspects of K^+ homeostasis and the specific molecular mechanisms of K^+ transport by pumps, channels, co-transporters, and through tight-junction proteins are unconstrained or debated. For example, structural, functional and computational studies of K^+ channels produce conflicting results as to whether the molecular mechanism of K^+ permeation is water mediated or occurs by direct knock-on of cations (Mironenko et al., 2021). In addition, while studies of gene expression in cells and tissues can be used to identify which K transporters are active, quantitative constraints on the fluxes of K^+ through the different types of transporters *in vivo* are non-existent.

In natural systems potassium is made up of two stable (potassium-39 and potassium-41) and one radioactive (potassium-40) isotope. The two stable isotopes of K, ^{39}K and ^{41}K, constitute 93.258% and 6.730% of the total, respectively, resulting in a ratio of $^{41}K/^{39}K$ in nature of ~0.07217. Recent advances in inductively coupled plasma mass spectrometry (ICP-MS) now permit the precise quantification of deviations from the terrestrial ratio resulting from the biogeochemical cycling of potassium in nature with a precision of 1 part in 10,000 (Wang and Jacobsen, 2016; Morgan et al., 2018). Here we apply this analytical tool to study K^+ homeostasis in three biological systems–aquatic green alga *Chlamydomonas reinhardtii* (*C. reinhardtii*), a suite of marine fish that include species that can tolerate a wide range in salinities (euryhaline) as well as those that have a restricted salinity range (stenohaline), and the terrestrial mammal *Rattus norvegicus* (*R. norvegicus*). The results in each system are interpreted as reflecting K^+ homeostasis under normal (optimal) growth conditions.

2 Materials and methods

2.1 C. reinhardtii cultures

The CMJ030 wild type strain was obtained from the Chlamydomonas culture collection www.chlamycollection.org). Tris Phosphate (TP) medium was prepared according to: Gorman, D.S, and R.P. Levine (1965) Proc. Natl. Acad. Sci. United States 54, 1665–1669. The culture at an initial density of 0.5×10^5 cells mL^{-1} was grown in TP under continuous illumination (100 μmol photons $m^{-2} s^{-1}$) and shaking for 4 days. Samples (in triplicate) containing 2×10^7 cells (~800 mg) were harvested and washed twice in 5 mM HEPES and 2 mM EDTA before collection and air-drying of the cell pellet. Pelletized cells (~30 mg) were digested in screw-capped teflon vials on a hot plate at elevated temperatures (~75°C) using a 5:2 mixture of HNO_3 (68–70 vol.%) and H_2O_2 (30 vol.%).

2.2 Euryhaline and stenohaline marine teleosts

Samples of teleost muscle tissue were sourced from fish markets (Nassau Seafood and Trader Joe's in Princeton, NJ and the Fulton Fish Market in Brooklyn, NY) and research cruises (NOAA NEFSC Bottom Trawl Survey, Fall 2015 and Spring 2015). All teleosts were caught in seawater which has a
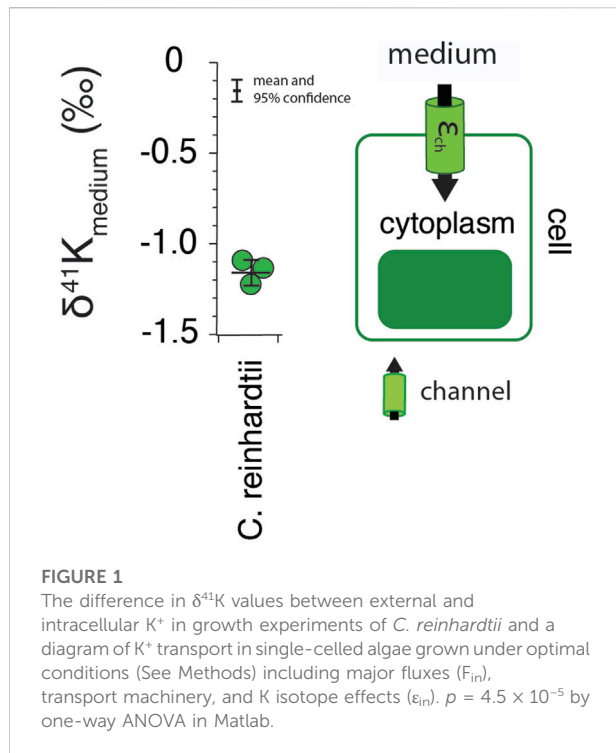
uniform $\delta^{41}K$ value of +0.12‰ relative to SRM3141a (Ramos et al., 2020). Samples of white dorsal muscle (100–3000 mg) were digested on a hot plate at elevated temperatures (~75°C) or in a high-pressure microwave system (MARS 6) using HNO_3 (68–70 vol.%) H_2O_2 (30 vol.%) in a ratio of 5:2. Major/minor element analyses for digested samples were carried out at Princeton University using a quadrupole inductively coupled plasma mass spectrometer (Thermo Scientific iCap Q). Concentrations and elemental ratios were determined using externally calibrated standards and average uncertainties (element/element) are ~10%.

2.3 R. norvegicus experiments

All rat experiments were approved by the Institutional Animal Care and Use Committees of the University of Southern California. Two series were conducted. Series #1: Male Wistar rats ($n = 3$, 250–275 g body weight, Envigo, Indianapolis, IN) were housed in a climate controlled (22–24°C) environment with a 12 h: 12 h light/dark cycle, and fed casein based normal K^+ diet TD.08267 (Envigo, Indianapolis, IN) and water *ad libitum* for 11 days. At day 8, rats were placed overnight into metabolic cages (Techniplast, Buguggiate, Italy) with food and water *ad libitum* for 16-h collection of urine and feces. On termination day (1:30–3:30p.m.), rats were anesthetized with an intramuscular (IM) injection of ketamine (80 mg/kg, Phoenix Pharmaceuticals, St. Joseph, MO) and xylazine (8 mg/kg, Lloyd Laboratories, Shenandoah, IA) in a 1:1 ratio. Through a midline incision, the liver, kidneys, heart, fat pads, and stomach (flushed of contents) were removed; blood was collected *via* cardiac puncture, spun down to separate plasma from RBCs. Then gastrocnemius, soleus, TA, and EDL skeletal muscles were dissected. All tissues were washed in ice-cold TBS to remove excess blood, weighed and snap frozen in liquid nitrogen. Series #2: Male Sprague Dawley rats ($n = 4$, 250–300 g, Envigo, Indianapolis, IN) were housed in a climate controlled (22–24°C) environment with a 12 h: 12 h light/dark cycle and fed grain-based vivarium chow (LabDiet 5001, labdiet.com). CSF extraction procedures are as reported previously (Noble et al., 2018). In brief, Rats were deeply anesthetized using a cocktail of ketamine 90 mg/kg, xylazine, 2.8 mg/kg, and acepromazine 0.72 mg/kg by intramuscular injection. A needle was lowered to below the caudal end of the occipital skull and the syringe plunger pulled back slowly, allowing the clear CSF to flow into the syringe. After extracting ~100–200 μL of CSF, the needle was raised quickly (to prevent suction of blood while coming out of the cisterna magna) and the CSF dispensed into a microfuge tube and immediately frozen in dry ice and then stored at -80°C until time of analysis. Following CSF extraction and decapitation, whole brains with 10–15 mm spinal cord extension were rapidly removed and immediately flash frozen and stored in -80°C until dissection into spinal cord, cerebrum, and cerebellum for subsequent digestion and K isotopic analysis.
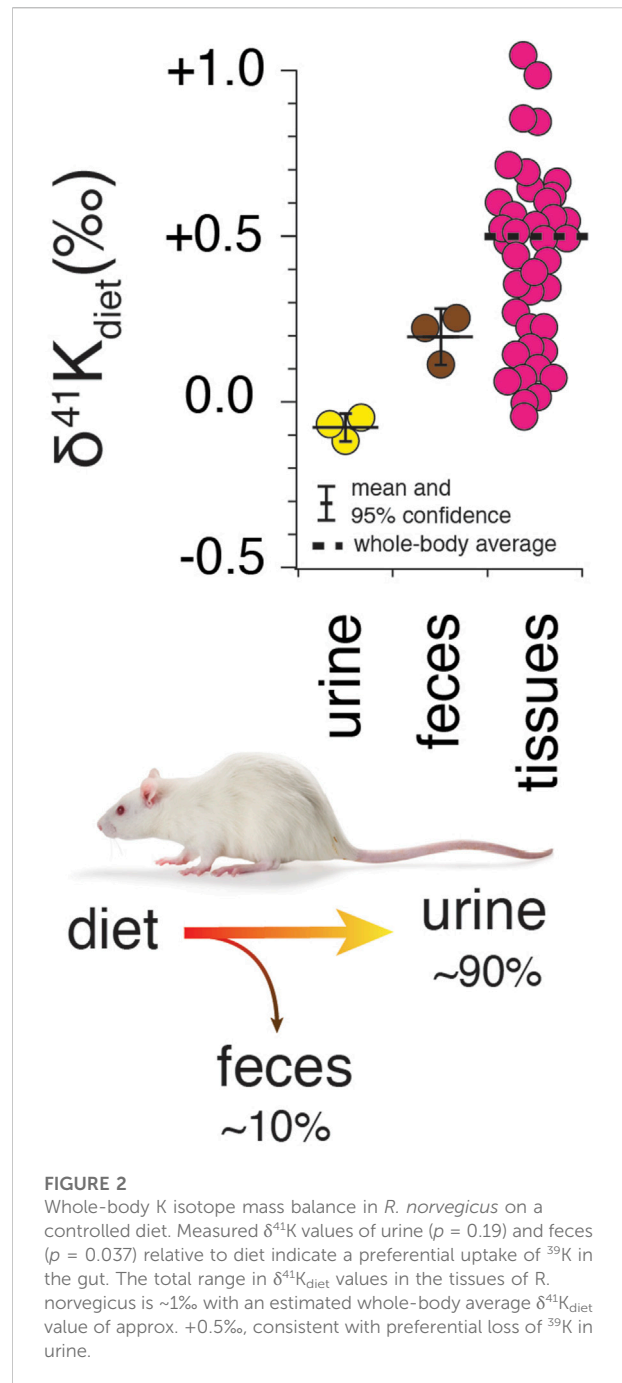
2.4 Ion chromatography and isotope ratio mass-spectrometry

K was purified for isotopic analyses using an automated high-pressure ion chromatography (IC) system. The IC methods utilized here followed those previously described in (Morgan et al., 2018; Ramos et al., 2018). Briefly, chemical separation of cations for high-precision isotopic analyses by MC-ICP-MS was performed using an automated Dionex ICS-5000 + ion chromatography (IC) system at Princeton University. Digested samples were dried down then diluted in 0.2% HNO_3 acid to ~10–20 ppm K and loaded onto a Dionex CS-16 cation exchange column at a rate of 1 ml/min with methanesulfonic acid (MSA) as eluent. Minimum sample sizes needed for both column chemistry and mass spectrometry were <5 μg of K and samples were run along with external standards in order to monitor the efficacy of column chemistry. External standards included a high-purity K solutions (SRM3141a), and the NIST K-feldspar standard SRM 70 b. Purified K solutions were allowed to dry overnight in PFA Teflon vials, redissolved in 200 μL of 16 N (70% v/v) trace-metal grade HNO_3 in order to eliminate any organics, then dried again prior to isotopic analysis. Purified K separates were diluted to ~1 ppm K in 2% trace-metal grade HNO_3 prior to isotopic analysis on a Thermo Scientific Neptune Plus multi-collector inductively coupled plasma mass spectrometer (MC-ICP-MS) at Princeton University. Measurement of K isotopic ratios by MC-ICP-MS is hindered by the large isobaric interferences on masses 39 and 41, due to ionization of the carrier gas (argon) and formation of argon hydrides ($^{38}ArH^+$ and $^{40}ArH^+$, respectively). Here, we use cold plasma (~600 W) settings, an Elemental Scientific Instruments (ESI) Apex Omega desolvating nebulizer, and high mass-resolution mode (M/ΔM ca. 10,000) to measure $^{41}K/^{39}K$ ratios on small (2–3 milli-amu) but flat peak shoulders. The instrument is tuned to optimize stability and sensitivity, with ~1 ppm K yielding voltages between 5 and 6 V on mass 39. Caution was taken to assure that samples matched standard concentrations (~1 ppm K) to within 5%, artifacts due to imbalances during analysis were corrected using high-purity K standards run at different ion intensities in the same analytical session, and the same batch of 2% HNO_3 was used to dilute both samples and standards in a single run. Instrumental mass-drift was corrected by applying the standard-sample-standard bracketing technique with high-purity KNO_3 as the bracketing standard solution. The accuracy of our chromatographic methods was verified by purifying and analyzing external standards (SRM3141a and SRM70 b) alongside unknown samples. Purified aliquots of K were analyzed in 2% HNO_3 for their isotopic compositions on a Thermo Scientific Neptune Plus multi-collector inductively coupled plasma mass spectrometer (MC-ICP-MS) at Princeton University, using previously published methods (Morgan et al., 2018; Ramos et al., 2020). The data are presented using standard delta notation in parts per thousand (‰).

FIGURE 1
The difference in $\delta^{41}K$ values between external and intracellular K^+ in growth experiments of *C. reinhardtii* and a diagram of K^+ transport in single-celled algae grown under optimal conditions (See Methods) including major fluxes (F_{in}), transport machinery, and K isotope effects (ϵ_{in}). $p = 4.5 \times 10^{-5}$ by one-way ANOVA in Matlab.

$$\delta^{41/39}K = \left(R^{41K/39K}_{sample} \Big/ R^{41K/39K}_{standard} - 1 \right) \cdot 10^3$$

where $R^{41K/39K}_{sample}$ is the ratio of $^{41}K/^{39}K$ in a sample and $R^{41K/39K}_{standard}$ is the $^{41}K/^{39}K$ of the standard). For plants the standard is the $^{41}K/^{39}K$ of the growth medium, whereas for marine teleosts it is the $^{41}K/^{39}K$ of seawater. For *R. norvegicus*, we report the data in one of two ways. To explore total body K^+ homeostasis we report the $^{41}K/^{39}K$ of K excretory losses normalized to the $^{41}K/^{39}K$ of the diet whereas to examine the partitioning of K isotopes between extracellular and intracellular compartments we report the $^{41}K/^{39}K$ of tissues relative to the $^{41}K/^{39}K$ of blood plasma or cerebrospinal fluid (CSF). K isotope fractionation factors are calculated as ratios of isotope ratios (e.g., $\alpha_{medium/cell} = [^{41}K/^{39}K_{medium}]/[^{41}K/^{39}K_{cell}]$) and reported as ϵ values (in ‰) where $\epsilon_{medium/cell} = \alpha_{medium/cell} - 1$. The external reproducibility of our protocols (chromatography and mass spectrometry) was determined through replicate measurements of international standards. Measured values of SRM70b, reported relative to SRM3141 ($\delta^{41}K_{SRM3141}$) are -0.57 ± 0.17‰ (2σ; N = 59), indistinguishable from published values (Wang and Jacobsen, 2016; Ramos et al., 2018; Ramos et al., 2020). For samples analyzed once (chromatography and mass spectrometry), reported errors are the 2σ uncertainties of the external standard. In cases where samples were analyzed multiple times, reported errors in are twice the standard error of the mean (2 S.E. or 95% confidence).

FIGURE 2
Whole-body K isotope mass balance in *R. norvegicus* on a controlled diet. Measured $\delta^{41}K$ values of urine ($p = 0.19$) and feces ($p = 0.037$) relative to diet indicate a preferential uptake of ^{39}K in the gut. The total range in $\delta^{41}K_{diet}$ values in the tissues of R. norvegicus is ~1‰ with an estimated whole-body average $\delta^{41}K_{diet}$ value of approx. +0.5‰, consistent with preferential loss of ^{39}K in urine.

3 Results

Results for the freshwater algae *C. reinhardtii* are shown in Figure 1. Measured $\delta^{41}K$ values of the whole cells are 1.2 ± 0.07‰ lower than the $\delta^{41}K$ value of the growth medium (0‰ by definition) (95% confidence; $p = 4.5 \times 10^{-5}$).

Results for *R. norvegicus* are shown in Figures 2–4. Figure 2 shows the measured $\delta^{41}K$ values of both urine and feces, normalized to the $\delta^{41}K$ value of the rat diet ($\delta^{41}K_{diet}$). A
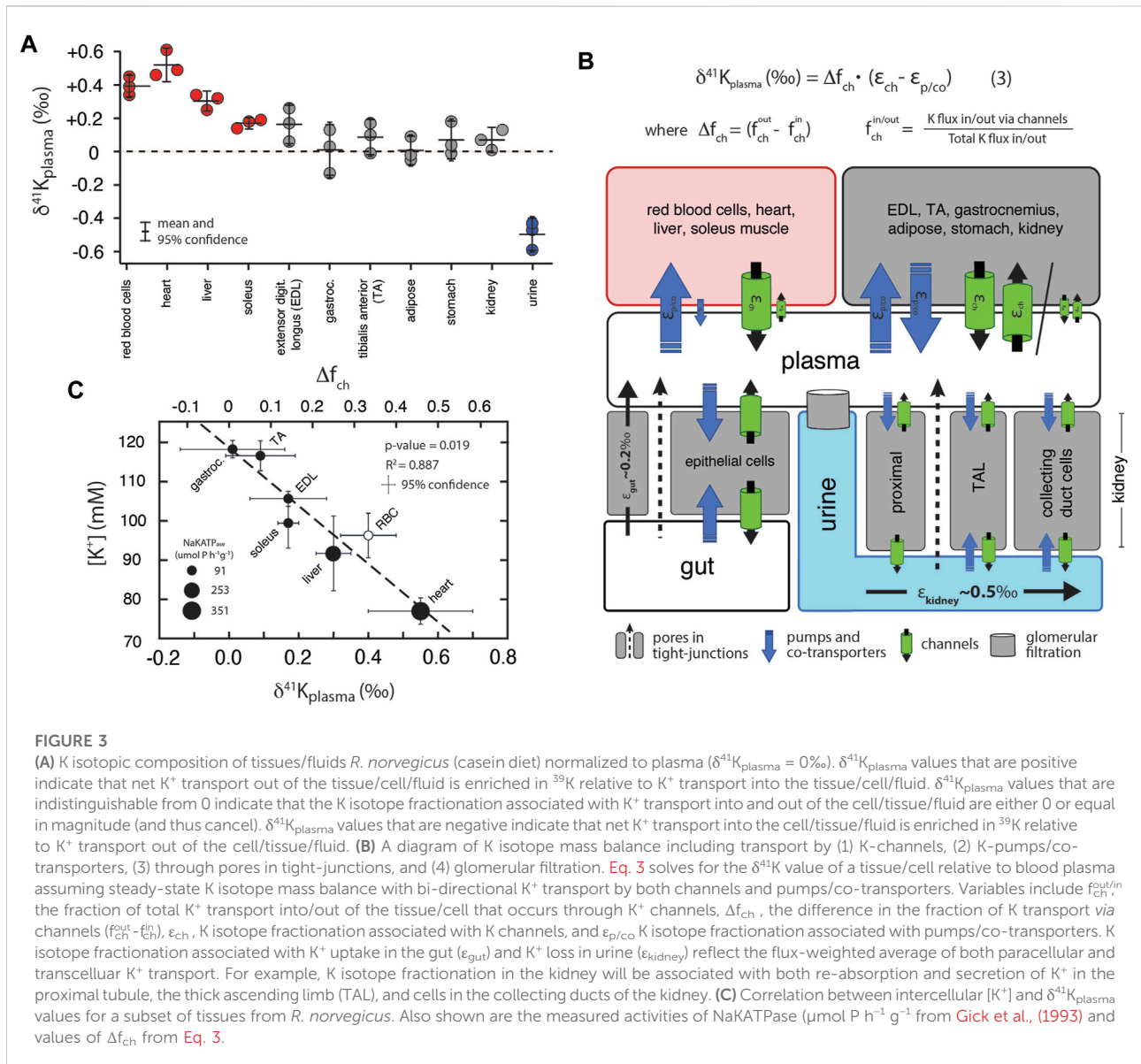
FIGURE 3
(A) K isotopic composition of tissues/fluids *R. norvegicus* (casein diet) normalized to plasma ($\delta^{41}K_{plasma}$ = 0‰). $\delta^{41}K_{plasma}$ values that are positive indicate that net K^+ transport out of the tissue/cell/fluid is enriched in ^{39}K relative to K^+ transport into the tissue/cell/fluid. $\delta^{41}K_{plasma}$ values that are indistinguishable from 0 indicate that the K isotope fractionation associated with K^+ transport into and out of the cell/tissue/fluid are either 0 or equal in magnitude (and thus cancel). $\delta^{41}K_{plasma}$ values that are negative indicate that net K^+ transport into the cell/tissue/fluid is enriched in ^{39}K relative to K^+ transport out of the cell/tissue/fluid. **(B)** A diagram of K isotope mass balance including transport by (1) K-channels, (2) K-pumps/co-transporters, (3) through pores in tight-junctions, and (4) glomerular filtration. Eq. 3 solves for the $\delta^{41}K$ value of a tissue/cell relative to blood plasma assuming steady-state K isotope mass balance with bi-directional K^+ transport by both channels and pumps/co-transporters. Variables include $f_{ch}^{out/in}$, the fraction of total K^+ transport into/out of the tissue/cell that occurs through K^+ channels, Δf_{ch}, the difference in the fraction of K transport *via* channels (f_{ch}^{out}-f_{ch}^{in}), ε_{ch}, K isotope fractionation associated with K channels, and $\varepsilon_{p/co}$ K isotope fractionation associated with pumps/co-transporters. K isotope fractionation associated with K^+ uptake in the gut (ε_{gut}) and K^+ loss in urine (ε_{kidney}) reflect the flux-weighted average of both paracellular and transcellular K^+ transport. For example, K isotope fractionation in the kidney will be associated with both re-absorption and secretion of K^+ in the proximal tubule, the thick ascending limb (TAL), and cells in the collecting ducts of the kidney. **(C)** Correlation between intercellular $[K^+]$ and $\delta^{41}K_{plasma}$ values for a subset of tissues from *R. norvegicus*. Also shown are the measured activities of NaKATPase (µmol P h^{-1} g^{-1} from Gick et al., (1993) and values of Δf_{ch} from Eq. 3.

positive $\delta^{41}K_{diet}$ value in feces (+0.19 ± 0.09‰, 95% confidence; p = 0.037; Figure 2) and slightly negative $\delta^{41}K_{diet}$ value in urine (-0.09 ± 0.10‰, 95% confidence; p = 0.1895) are consistent with preferential net uptake of ^{39}K relative to ^{41}K across the gut epithelium.

Figure 3A shows measurements of K isotopes of various tissues in *R. norvegicus* (except brain tissues) normalized to the $\delta^{41}K$ value of the blood plasma ($\delta^{41}K_{plasma}$), as this represents the extracellular K concentration bathing the tissues. The overall range in $\delta^{41}K_{plasma}$ values between different tissues and fluids is ~1‰; $\delta^{41}K$ values of the following tissues are elevated in ^{41}K relative to blood plasma (positive $\delta^{41}K_{plasma}$ values): red blood cells (+0.40 ± 0.08‰, p = 0.005), heart (+0.55 ± 0.15‰, p = 0.0047), liver (+0.30 ± 0.05‰, p =

0.01), and soleus muscle (+0.17 ± 0.03‰, p = 0.05). In another category are tissues with $\delta^{41}K_{plasma}$ values that are statistically indistinguishable from zero: kidneys (+0.07 ± 0.07‰, p = 0.31), adipose tissue (+0.01 ± 0.08‰, p = 0.92), extensor digitorum longus (EDL, +0.17 ± 0.11‰, p = 0.099) gastrocnemius (+0.01 ± 0.15‰, p = 0.92), and tibialis anterior (TA, +0.09 ± 0.1‰, p = 0.30). Finally, urine is characterized by a $\delta^{41}K_{plasma}$ value that is negative (-0.50 ± 0.10‰, p = 0.0019) indicating preferential enrichment of ^{39}K relative to blood plasma. Figure 3B is a diagram of K isotope mass balance between internal tissues in *R. norvegicus* and Figure 3C shows the correlation between measured $\delta^{41}K_{plasma}$ values, the concentration of K^+ (in mM) in the tissue, and the activity of NaKATPase (Gick et al., 1993).
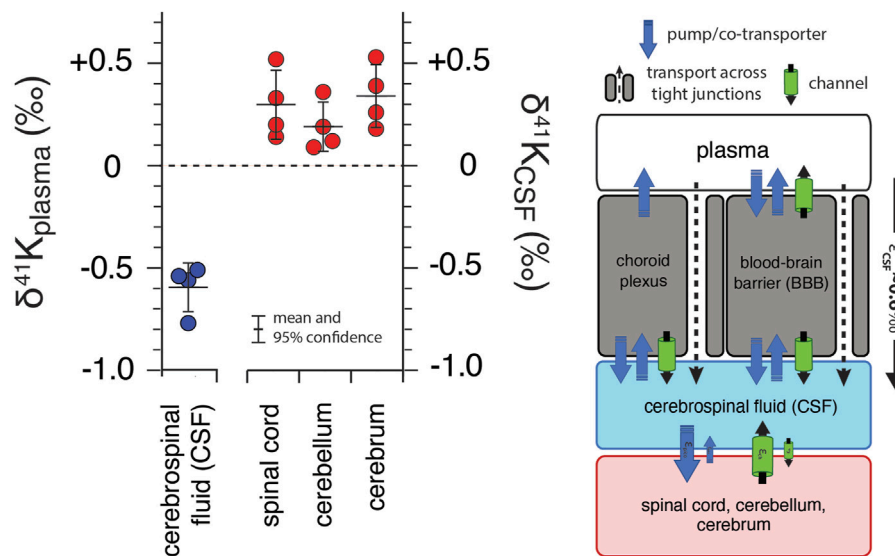
FIGURE 4
K isotopic composition of cerebrospinal fluid from *R. norvegicus* raised on a controlled diet (vivarium chow) normalized to blood plasma ($\delta^{41}K_{plasma}$ = 0‰) and brain tissues normalized to cerebrospinal fluid ($\delta^{41}K_{CSF}$ = 0‰) together with a diagram of K homeostasis across the choroid plexus and blood brain barrier (BBB) from Hladky and Barrand (2016) including transport by (1) K-channels, (2) K-pumps/co-transporters, and (3) transcellularly through pores in tight-junctions. $\delta^{41}K_{CSF}$ values that are positive indicate that net K transport out of brain tissues (spinal cord, cerebellum, and cerebrum) and into CSF is enriched in ^{39}K relative to K transport from CSF into these tissues. The negative $\delta^{41}K_{plasma}$ values for CSF indicate that net K transport into CSF from blood plasma is enriched in ^{39}K relative to K transport from CSF to blood plasma and reflects the flux-weighted average of the transporters that dominate K^+ exchange across both the choroid plexus and BBB.

Figure 4 shows of K isotopes of brain tissues, normalized to CSF ($\delta^{41}K_{CSF}$) and CSF normalized to blood plasma. Brain tissues are elevated in ^{41}K relative to CSF (positive $\delta^{41}K_{CSF}$ values): cerebrum (+0.34 ± 0.15‰, p = 0.012), spinal cord (+0.30 ± 0.17‰, p = 0.026), and cerebellum (+0.21 ± 0.11‰, p = 0.037). In contrast, CSF (-0.59 ± 0.12‰, p = 6.2 × 10^{-5}) is characterized by a negative $\delta^{41}K_{plasma}$ value.

Results for white muscle tissue from a suite of stenohaline and euryhaline marine fish, reported relative to the $^{41}K/^{39}K$ of seawater ($\delta^{41}K_{seawater}$ = 0‰) are shown in Figure 5A. The total range in muscle $\delta^{41}K$ values is ~2‰ (+1‰ to -1‰). Stenohaline species including *Gadus morhua* (Atlantic Cod), *Peprilus striacanthus* (Butterfish), *Xiphias gladius* (Swordfish), *Pseudopleuronectes americanus* (Winter Flounder), and *Hippoglossus stenolepis* (Pacific Halibut) are characterized by $\delta^{41}K_{seawater}$ values that are uniformly negative whereas the euryhaline species *Oncorhynchus kisutch* (Coho Salmon), *Oncorhynchus tshawytscha* (King Salmon), and *Oncorhynchus nerka* (Sockeye Salmon) are characterized by $\delta^{41}K_{seawater}$ values that are close to zero or positive. When species are grouped by salinity tolerance, average measured $\delta^{41}K_{seawater}$ values of the two groups are -0.58 ± 0.09‰, and 0.29 ± 0.18‰ for stenohaline and euryhaline species, respectively (95% confidence; p = 1.4 × 10^{-10}). Figure 5B shows a diagram of external and internal K isotope mass balance in marine fish.

4 Discussion

The shared machinery of K^+ transport across the domains of life suggests that the variability in K isotopes observed in biological systems can be reduced to a consideration of 1) how different classes of K^+ transporters—tight junctions, channels, pumps, and co-transporters - discriminate between ^{39}K and ^{41}K and 2) how these transporters are assembled into a homeostatic system. The extent to which K^+ transporters fractionate K isotopes will, in turn, depend on the mechanics and selectivity of the transporter and whether the binding of dissolved K^+ to transporter is the rate-limiting step. In particular, K^+ channels and pores in tight-junction proteins are both associated with selective and rapid (near the limit of diffusion) transport of K^+ where the rate-limiting step is the binding of dissolved K^+ to the transporter/selectivity filter. These conditions favor kinetic isotope effects which may arise from either partial or full desolvation of K^+ as it binds to the selectivity filter (Berneche and Roux, 2003; Yu et al., 2010; Hofmann et al., 2012; Kopec et al., 2018), differences in ionic radius of ^{39}K and ^{41}K [size selectivity (Christensen et al., 2018)], or some combination of the two. Critically, the magnitude of the kinetic isotope effects associated with both desolvation and/or size selectivity appear to be large, with estimates from laboratory experiments and molecular dynamic simulations ranging from ~1 to 2.7‰ (Hofmann et al., 2012).
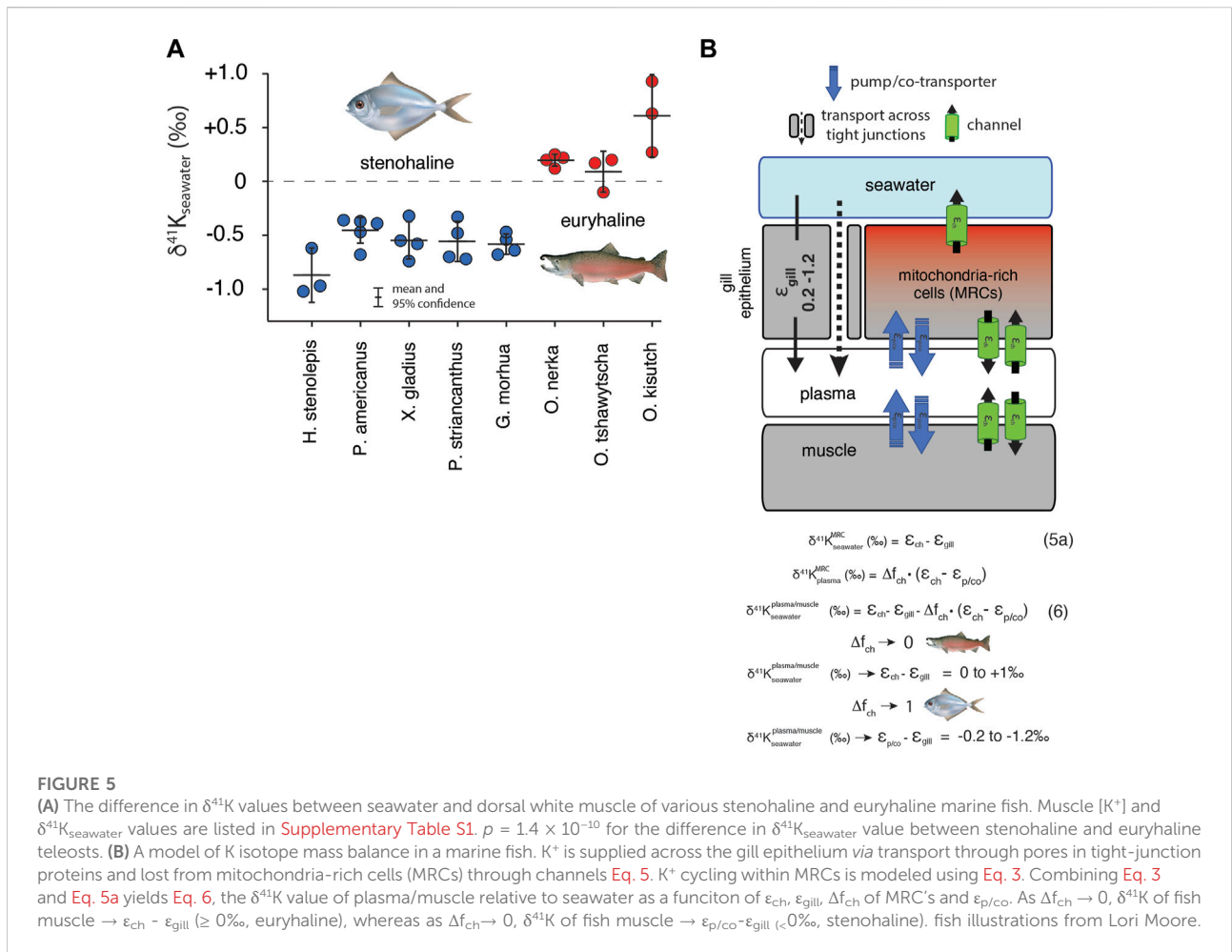
FIGURE 5
(A) The difference in $\delta^{41}K$ values between seawater and dorsal white muscle of various stenohaline and euryhaline marine fish. Muscle [K$^+$] and $\delta^{41}K_{seawater}$ values are listed in Supplementary Table S1. $p = 1.4 \times 10^{-10}$ for the difference in $\delta^{41}K_{seawater}$ value between stenohaline and euryhaline teleosts. **(B)** A model of K isotope mass balance in a marine fish. K$^+$ is supplied across the gill epithelium *via* transport through pores in tight-junction proteins and lost from mitochondria-rich cells (MRCs) through channels Eq. 5. K$^+$ cycling within MRCs is modeled using Eq. 3. Combining Eq. 3 and Eq. 5a yields Eq. 6, the $\delta^{41}K$ value of plasma/muscle relative to seawater as a funciton of ε_{ch}, ε_{gill}, Δf_{ch} of MRC's and $\varepsilon_{p/co}$. As $\Delta f_{ch} \to 0$, $\delta^{41}K$ of fish muscle $\to \varepsilon_{ch} - \varepsilon_{gill}$ ($\geq$ 0‰, euryhaline), whereas as $\Delta f_{ch} \to 0$, $\delta^{41}K$ of fish muscle $\to \varepsilon_{p/co} - \varepsilon_{gill}$ (<0‰, stenohaline). fish illustrations from Lori Moore.

In contrast to channels and pores in tight-junction proteins, transport of K$^+$ by pumps and co-transporters is relatively slow [per unit transporter, (Roux, 2017)], requires the simultaneous binding of multiple ions (e.g., 2 K$^+$ ions in the case of Na,K-ATPase), and is associated with mechanisms of self-correction that prevent the pump cycle from proceeding if incorrect ions bind to the ion pocket (Rui et al., 2016). As a result, although the binding of K$^+$ to the active site of a pump or cotransporter may also involve desolvation, it is not the rate-limiting step in K$^+$ transport. In this case, the isotopic composition of K$^+$ that is transported by pumps and co-transporters may reflect isotopic equilibration between K+in the ion pocket and the fluid due to the longer residence time of K$^+$ in the ion pocket prior to occlusion. As equilibrium K isotope effects tend to be small (Li et al., 2017; Ramos et al., 2018; Zeng et al., 2019), we hypothesize that K$^+$ transport by pumps and co-transporters will be associated with less isotopic fractionation.

In the following sections we show how our results for the three studied biological systems (algae, fish, mammals) can be interpreted within a single framework where K$^+$ transport by channels and pores in tight-junction proteins is associated with large (kinetic) K isotope effects whereas K$^+$ transport by pumps and/or co-transporters is associated with smaller (equilibrium) K isotope effects. In simple biological systems (e.g., single celled alga) linking K isotope fractionation to the machinery of K$^+$ transport is relatively straightforward due to the small number of pathways involved and the unidirectional nature of K$^+$ transport. In more complex biological systems (e.g., higher plants, fish, and mammals) discerning transporter-specific fractionation of K isotopes is more difficult for at least two reasons. First, our understanding of K homeostasis at both the tissue and organism level is incomplete. Second, our measured K isotopic differences (e.g., between plasma/CSF/seawater and tissue) only provide information on net K isotope fractionation associated with bi-directional K$^+$ transport at steady-state. In spite of these limitations, our results support a framework for K isotope fractionation in biological systems that can provide new quantitative insights into the mechanisms of K$^+$ transport and the dynamics of K homeostasis.

4.1 Algae

As an essential macronutrient in all plants and the most abundant cation in the cytoplasm, K^+ contributes to electrical neutralization of anionic groups, membrane potential and osmoregulation, photosynthesis, and the movements of stomata (Gierth and Mäser, 2007; Marchand et al., 2020). It is well-established that K^+ channels play prominent roles in K^+ uptake (Lebaudy et al., 2007). For example, under normal growth conditions {$[K^+]_{ext}$ ~1 mM; (Epstein et al., 1963; Kochian and Lucas, 1982; Malhotra and Glass, 1995)} K^+ uptake in plants is dominated by transport *via* inward-rectifying K^+ channels electrically balanced by the ATP-driven efflux of H^+ (Hirsch et al., 1998; Britto and Kronzucker, 2008). Considered in this context our results for whole cells of *C. reinhardtii* can be interpreted as reflecting K isotope fractionation associated with uptake *via* K^+ channels ($\varepsilon_{in} = \delta^{41}K_{medium} - \delta^{41}K_{Cell} =$ ~1.2‰; Figure 1). Although we cannot guarantee that K uptake occurs exclusively *via* K^+ channels, this result represents our best estimate of a transporter-specific K isotope effect (ε_{ch}). The magnitude of this effect is smaller than modeled estimates of the kinetic isotope effect associated with ion desolvation (Hofmann et al., 2012) and of the same order as hypothesized kinetic isotope effects associated with size-selectivity (Christensen et al., 2018).

4.2 Higher plants

Our result for K isotope fractionation associated with K^+ uptake in *C. reinhardtii* is similar in sign, though somewhat larger in magnitude, than the K isotope effect associated with K^+ uptake estimated by Christensen et al. (2018) in experiments involving higher plants. Those authors analyzed the $\delta^{41}K$ values of the roots, stems, and leaves of *Triticum aestivum* (wheat), *Glycine max* (soy) and *Oryza sativa* (rice) grown under hydroponic conditions and observed systematic differences in the $\delta^{41}K$ value of the different reservoirs. In particular, roots, stems, and leaves exhibited increasingly negative $\delta^{41}K$ values (Supplementary Figure S1). Compared to the freshwater alga *C. reinhardtii*, quantifying transport-specific K isotope effects in higher plants is more complex as the $\delta^{41}K$ value of each individual compartment (root, stem, leaf) reflects a balance between isotopic sources and sinks [e.g., the $\delta^{41}K$ value of the root will depend on K isotope effects associated with both net K^+ uptake as well as translocation and recycling]. Using a model of K isotope mass balance that includes assumptions regarding plant growth and the partitioning of K^+ fluxes between translocation and recycling, Christensen et al. (2018) estimated large K isotope effects for uptake (ε_{in} ~0.7–1.0‰) and translocation from root to stem (~0.6‰), but smaller isotopic effects (0–0.2‰) for translocation of K^+ from stem to leaf and recycling of K^+ from leaf to root. Interestingly, in addition to their important

role in K^+ uptake, K^+ channels have also been shown to be involved in translocation [root to stem; (Gaymard et al., 1998)] providing a potential explanation for the relatively large K isotope effect observed by Christensen et al. (2018) for this process. In contrast, translocation and recycling of K^+ from leaf to root, a process that also involves K^+ channels (Lacombe et al., 2000; Pilot et al., 2001), does not appear to result in significant fractionation of K isotopes. This could be due to the increased importance of other types of K^+ transporters in this process, a reduction in the expression of K isotope fractionation by channels due to rapid internal recycling of K^+ between stem and leaf (compared to K^+ transport from root to stem), or some combination of the two.

4.3 Terrestrial mammals

K^+ homeostasis in terrestrial mammals reflects the balance between K^+ gained from diet and K^+ lost in urine and feces (Figure 2, Figure 3A). This balance is largely achieved by the kidneys and colon, which possess a remarkable ability to sense a change in K^+ in the diet and then appropriately adjust K^+ loss in response. ECF (which includes blood plasma), the reservoir through which internal K^+ is exchanged, represents only 2% of total body K^+. Though small, this reservoir is tightly regulated to maintain membrane potential as indicated by the narrow range of normal ECF $[K^+]$ (~ 3.5–5 mEq/L) (Boron and Boulpaep, 2005; McDonough and Youn, 2017). Of the remaining 98% of total body K^+, 75% resides in muscle tissues ($[K^+]$ ~ 130 mEq/L) and 23% in non-muscle tissues. Some tissues, particularly skeletal muscle, are critical to K^+ homeostasis by providing a buffering reservoir of K^+ that can take up K^+ after a meal and altruistically donate K^+ to ECF to maintain blood plasma levels during fasting (McDonough and Youn, 2017). Cerebrospinal fluid (CSF), the body fluid that surrounds the brain and spinal cord of all vertebrates, merits special mention as its K^+ content is even more tightly regulated than ECF (Bradbury and Davson, 1965).

4.3.1 External K isotope mass balance in terrestrial mammals

Roughly ~80–90% of K in the diet is lost in urine with the remainder lost in feces (Agarwal et al., 1994). Uptake of K^+ across gut endothelial cells occurs largely paracellularly through pores in tight-junction proteins like claudin-15 (Garcia-Hernandez et al., 2017) as a result of the transmucosal electrical potential difference (Barnaby and Edmonds, 1969). However, transcellular K^+ uptake (*via* pumps) and secretion (*via* channels) and transcellular secretion has also been shown to occur in gut epithelial cells (Foster et al., 1984; Tsai et al., 2017). As a result, K isotope fractionation associated with net K uptake in the gut will reflect the flux-weighted average of the K isotope fractionation associated with both transcellular and paracellular

K$^+$ transport. The observation that feces is characterized by a positive $\delta^{41}K_{diet}$ value and urine with a slightly negative $\delta^{41}K_{diet}$ value (Figure 2) indicates that the net K isotope effect associated with K uptake under these conditions (ε_{gut}) is ~0.2‰ (Figure 3B). Relative to the diet, internal tissues of *R. norvegicus* exhibit a 1‰ range from -0.04‰ for the cerebellum to +1.05‰ for the heart (Figure 2). Assuming an internal K$^+$ distribution that is 75/15/10 muscle/adipose/other tissues, a reasonable average whole-body $\delta^{41}K_{diet}$ value of *R. norvegicus* is ~+0.5‰. As net uptake of K$^+$ in the gut prefers ^{39}K, the elevated average whole-body $\delta^{41}K_{diet}$ of *R. norvegicus* requires that there be even greater K isotope fractionation (favoring ^{39}K) associated with K$^+$ loss in the urine (see below).

4.3.2 Internal K isotope mass balance in terrestrial mammals

As shown in Figures 3A, 4, measured $\delta^{41}K$ values of the 16 different tissues and fluids analyzed in *R. norvegicus* fall into 3 distinct categories relative to ECF ($\delta^{41}K_{plasma}$ or $\delta^{41}K_{CSF}$): those with positive $\delta^{41}K_{plasma/CSF}$ values (red blood cells, heart, liver, soleus muscle and brain tissues), those with $\delta^{41}K_{plasma/CSF}$ values that are close to 0 (stomach, adipose tissue, kidney, gastrocnemius, EDL and TA muscles), and those with negative $\delta^{41}K_{plasma/CSF}$ values (urine and CSF).

The timescale for K$^+$ turnover in the studied tissue/cell/fluid reservoirs is rapid [e.g., 0.9–10%/min; (Terner et al., 1950; Jones et al., 1977)]. As a result, for all measured tissues/cells, the $\delta^{41}K$ values in Figure 3A can be interpreted as reflecting steady-state K isotope mass balance between the tissue/cell/fluid and the relevant fluid (blood plasma/ECF or CSF). At isotopic steady-state, the $\delta^{41}K$ value of K$^+$ entering the reservoir must equal to $\delta^{41}K$ value of K$^+$ leaving the reservoir. As a result, reservoirs with $\delta^{41}K_{plasma/CSF}$ values that differ from 0‰ require that net K$^+$ transport in one direction results in greater fractionation of K isotopes than net K$^+$ transport in the opposite direction. For example, reservoirs with positive $\delta^{41}K_{plasma}$ values including red blood cells, heart, liver, and soleus require that K$^+$ transport from ICF to plasma or ECF is associated with a larger K isotope effect than K$^+$ transport from ECF to ICF. The same relationship is observed between brain tissues and CSF (Figure 4). Similarly, reservoirs with $\delta^{41}K_{plasma}$ values that are close to 0‰ require that net K$^+$ transport in both directions does not fractionate K isotopes, i.e., the isotope effects must be of equal magnitude and sign and cancel. These include kidney, adipose tissue, stomach, and gastrocnemius and TA muscles. Finally, the negative $\delta^{41}K_{plasma}$ values for CSF requires that net K$^+$ transport from ECF to CSF through the choroid plexus and blood brain barrier (BBB) is characterized by a K isotope effect that is ~0.6‰ greater than the K isotope effect associated K$^+$ transport from CSF to ECF (Figure 4).

Quantitatively linking the observed isotopic differences between ECF and ICF of various tissues/cells to the machinery of K$^+$ homeostasis in complex biological systems is complicated by both an incomplete understanding of the machinery involved and limitations of steady-state isotopic mass balance. In particular, although much is known about the identity and molecular structure of the machinery that maintains K$^+$ homeostasis, quantitative information on how each transporter contributes to the gross fluxes of K$^+$ between ICF and ECF at the resting membrane potential is lacking. For example, in red blood cells, probably the best understood with regard to the machinery of K$^+$ homeostasis due to the fundamental role it plays in the regulation of cell volume and longevity (Tosteson and Hoffman, 1960), elevated intercellular K$^+$ is believed to be maintained by a 'pump-leak' mechanism where the pump is Na,K-ATP$_{ase}$ and the leak is K$^+$ channels (Gardos, 1958). However, red blood cells also show activity for co-transporters such as NKCC (Sachs, 1971; Duhm, 1987) and KCC (Franco et al., 2013), as well as inward-rectifying K$^+$ channels (Hibino et al., 2010), and exactly how much K$^+$ is transported by which transporter at the resting membrane potential is not well known.

In order to evaluate whether or not differences in measured $\delta^{41}K_{plasma}$ values reflect quantitative differences in K$^+$ fluxes through various transporters, we developed a generic model of K homeostasis (Figure 3B) that assumes 1) the tissue/cell is at the resting membrane potential and K is at isotopic steady-state between ECF and ICF, 2) all channels fractionate K isotopes identically (ε_{ch}), 3) all pumps and co-transporters fractionate K isotopes identically ($\varepsilon_{p/co}$), and 4) pumps, co-transporters, and channels may transport K$^+$ in either direction ($F^{in}_{p/co}$; $F^{out}_{p/co}$; F^{in}_{ch}, and F^{out}_{ch}):

$$F^{in}_{p/co} + F^{in}_{ch} = F^{out}_{p/co} + F^{out}_{ch} \qquad (1)$$

$$\begin{aligned}
\left(\delta^{41}K_{ECF} - \varepsilon_{p/co}\right) \cdot F^{in}_{p/co} & \\
+ \left(\delta^{41}K_{ECF} - \varepsilon_{ch}\right) \cdot F^{in}_{ch} &= \left(\delta^{41}K_{ICF} - \varepsilon_{p/co}\right) \cdot F^{out}_{p/co} \\
&+ \left(\delta^{41}K_{ICF} - \varepsilon_{ch}\right) \cdot F^{out}_{ch}
\end{aligned} \qquad (2)$$

where ε_{ch}, and $\varepsilon_{p/co}$ are the K isotope fractionation factors associated with channels and pumps/co-transporters, respectively. Solving for the $\Delta\delta^{41}K_{plasma}$ value of the ICF ($\delta^{41}K_{ICF} - \delta^{41}K_{ECF}$) yields:

$$\delta^{41}K_{plasma}\,(‰) = \Delta f_{ch} \cdot \left(\varepsilon_{ch} - \varepsilon_{p/co}\right) \qquad (3)$$

where $\Delta f_{ch} = f^{out}_{ch} - f^{in}_{ch}$, $f^{in/out}_{ch} = F^{in/out}_{ch}/(F^{in/out}_{ch} + F^{in/out}_{p/co})$. Assuming, based on our results for *C. reinhardtii*, that $\varepsilon_{ch} \sim 1.2‰$ and speculating, based on analogues with equilibrium K isotope effects associated with mineral precipitation in aqueous systems (Li et al., 2017; Ramos et al., 2018; Zeng et al., 2019), that $\varepsilon_{p/co} \sim 0‰$, reduces Eq. 1 to:

$$\delta^{41}K_{plasma}\,(‰) = 1.2 \cdot \Delta f_{ch} \qquad (4)$$

As $f_{ch}^{in/out}$ represent fractions of a flux, the value of Δf_{ch} is bounded at ±1; +1 representing a perfect "pump-leak" mechanism, -1 representing a perfect "leak-pump" mechanism, and 0 consistent with either a "pump-pump" or "leak-leak" mechanism. Accordingly, $\Delta\delta^{41}K_{plasma}$ values are bounded at ±1.2‰, with +1.2‰ representing a perfect "pump-leak" mechanism, -1.2‰ representing a perfect "leak-pump" mechanism, and 0‰ representing either a "pump-pump" or "leak-leak" mechanism. The observation that the $\Delta\delta^{41}K_{plasma}$ values of all internal reservoirs are ≥ 0 suggests that $\Delta f_{ch} \geq 0$, a result that is qualitatively consistent with the idea of elevated intercellular K^+ being maintained by a "pump-leak" mechanism. However, $\delta^{41}K_{plasma}$ values of the analyzed reservoirs also exhibit a considerable range, from ~0‰ for many skeletal muscles to +0.55‰ for the heart. In the context of Eq. 1, these differences can be explained by an increase in the relative importance of K^+ loss via channels. Skeletal muscles appear to maintain K homeostasis by something closer to a "pump-pump" or "leak-leak" mechanism whereas red blood cells, the liver and the heart approach ~50% of a perfect "pump-leak" mechanism.

Two lines of evidence provide additional independent support for our interpretation of $\delta^{41}K_{plasma}$ values as quantitative indicators of the relative importance of K^+ loss from ICF via channels (Eq. 3). First, measured $\delta^{41}K_{plasma}$ values are correlated with the activity of NaKATPase (umol Pi/h per g tissue) in tissues where this activity is related to the maintenance of intercellular $[K^+]$. In particular, NaKATPase activity ranges from 91 ± 15 in skeletal muscles, to 253 ± 8 in the liver, and 351 ± 23 in the heart (Gick et al., 1993). All else held constant, higher NaKATPase activity (K^+ sources to the ICF via pumps) will lower f_{ch}^{in} and increase Δf_{ch}, in agreement with observations. Second, measured $\delta^{41}K_{plasma}$ values also correlate with intercellular $[K^+]$ (Figure 4C). Because intercellular $[K^+]$ reflects the balance between K^+ sources and sinks one possible explanation for lower intercellular $[K^+]$ is a reduction in K^+ supply and/or an increase in K^+ loss. As K^+ supply from NaKATPase increases (see above), the most likely alternative explanations are less K^+ supply from inward rectifying K^+ channels and/or more K^+ loss via outward rectifying K^+ channels. Both of these processes increase Δf_{ch} and result in higher $\delta^{41}K_{plasma}$ values, again in agreement with observations.

4.3.2.1 Urine

Unlike the internal K^+ reservoirs discussed above, all of which are interpreted as independent homeostatic systems at isotopic steady-state with respect to ECF (plasma), the loss of K^+ through the urine represents the end product of a series of steps each of which may contribute to the observed net K isotope fractionation (e.g., Figure 3B; ε_{kidney} ~ 0.50‰). These are 1) glomerular filtration, 2) reabsorption and secretion along the proximal tubule and the thick ascending limb of the loop of Henle, and 3) secretion and reabsorption by principal and intercalated collecting duct cells. Although a detailed

description of the potential K isotope effects associated with each step is beyond the scope of this manuscript, a brief description follows. Glomerular filtration is not expected to fractionate K isotopes as the slit diaphragms freely filter ions and small molecules. A large fraction (~85%) of the filtered K^+ is subsequently reabsorbed via both paracellular and transcellular routes in the proximal tubule and thick ascending limb (TAL). The residual K^+ is passed along to the collecting ducts where K^+ is added or further reabsorbed, depending on systemic K homeostasis, prior to excretion as urine. The addition of K^+ in the collecting ducts occurs transcellularly, via ROMK channels in principal cells and BK channels in intercalated cells (McDonough and Youn, 2017). Although we expect K^+ channels to be associated with a large K isotope effect (ε_{ch} = 1.2‰), the extent to which this determines the $\delta^{41}K_{plasma}$ value of urine depends on 1) the $\delta^{41}K_{plasma}$ value of the residual K^+ exiting the TAL (after reabsorption but before secretion) and 2) internal K cycling within the principal and intercalated cells (e.g., Eq. 3). The observation that ε_{kidney} is only ~ 0.50‰ suggests that either the residual K^+ exiting the TAL has an elevated $\delta^{41}K_{plasma}$ value due to preferential removal of ^{39}K during reabsorption and/or the $\delta^{41}K_{plasma}$ value of ICF in principal and intercalated cells elevated, for example due to high values of Δf_{ch}.

4.3.2.2 Cerebrospinal fluid

K^+ in CSF reflects a balance between paracellular and transcellular K^+ transport across endothelial cells at the blood-brain-barrier (BBB) and paracellular K^+ transport of across epithelial cells of the choroid plexus (Hladky and Barrand, 2016). Gross fluxes of K^+ into the brain across the BBB are 4x larger than those associated with the choroid plexus (Katzman et al., 1965), suggesting that the observed net K isotope effects may be largely due to fractionation associated with transport across the BBB. However, K^+ transport from ECF to CSF through the choroid plexus is thought to occur by paracellular routes through pores in tight junctions (Figure 4), a process that we expect to fractionate K isotopes and thus may contribute to the observed negative $\delta^{41}K_{plasma}$ values for CSF. With regards to K^+ transport across the BBB, both paracellular (through tight-junction pores) and transcellular (through BBB endothelial cells) routes may be important (Hladky and Barrand, 2016). Again, we expect paracellular K^+ transport through tight junction pores to be associated with a larger K isotope effect whereas any K isotope effects associated with transcellular transport will depend on the internal cycling of K^+ (and associated isotope effects) within endothelial BBB cells (pumps, (Betz et al., 1980); co-transporters, (Foroutan et al., 2005); and channels, (Van Renterghem et al., 1995)). Overall, the observation of large K isotope fractionation associated with the transport of K^+ from plasma to CSF (Figure 5; ε_{CSF} = 0.59 ± 0.12‰) requires that either 1) there is a large K isotope effect associated with transcellular K^+ transport across endothelial BBB cells or 2) transport of K^+ from plasma to CSF is dominated by

paracellular routes in both the choroid plexus and across the BBB.

4.4 Stenohaline and euryhaline marine fish

K⁺ homeostasis in both euryhaline and stenohaline marine fish is linked to ionic and osmotic regulation (Figure 5). While K⁺ sources include ingestion of seawater and diet (Hickman Jr, 1968), by far the largest K⁺ source is transport across the gills (Maetz, 1969), which are permeable to monovalent cations (Na⁺, K⁺) and anions (Cl⁻). Fish balance this salt intake by actively secreting Na⁺, K⁺, and Cl⁻ through mitochondria-rich cells (MRCs) of the gills and paracellularly through tight-junction proteins (claudins) in the gill epithelium (Evans et al., 2005; Kolosov et al., 2013). K⁺ loss is not well-understood but recent discoveries of apical ROMK channels indicate that transcellular secretion through MRCs is likely an important pathway (Furukawa et al., 2012). Both stenohaline and euryhaline marine fish possess this capability but euryhaline marine fish have evolved the ability to adapt this machinery to a wide range of water salinities by adjusting expression of ROMK and tight junction claudins (Furukawa et al., 2012; Kolosov et al., 2013; Furukawa et al., 2014; Furukawa et al., 2015).

In seawater adapted stenohaline and euryhaline marine fish, K⁺ homeostasis can be approximated as a balance between gain of K⁺ across tight-junctions in the gill epithelium and loss of K⁺ through apical ROMK channels in MRCs (Figure 5B). Other potential sources and sinks of K⁺ including the ingestion of seawater, diet, and excretion are either small compared to the fluxes of K⁺ across the gills (Maetz, 1969) or transient in nature and unlikely to explain the systematic difference we observe between the $\delta^{41}K_{seawater}$ values of stenohaline and euryhaline fish. Furthermore, as most of the total K⁺ content of fish resides in muscle tissue, the $\delta^{41}K_{seawater}$ value of the muscle can be used as a reasonable approximation of the $\delta^{41}K_{seawater}$ value of the whole organism (Figure 5B). At steady-state ($F_{gill}^{in} = F_{MRC}^{out}$), the $\delta^{41}K_{seawater}$ value of the whole organism will reflect the balance between K isotope fractionation associated with K⁺ sources (paracellular transport across the gills, ε_{gill}) and K⁺ sinks (transcellular transport through ROMK channels in MRCs, ε_{ch}):

$$\left(\delta^{41}K_{seawater} - \varepsilon_{gill}\right)\cdot F_{gill}^{in} = \left(\delta^{41}K_{MRC} - \varepsilon_{ch}\right)\cdot F_{MRC}^{out} \quad (5)$$

which reduces to:

$$\delta^{41}K_{seawater}^{MRC} = \left(\varepsilon_{ch} - \varepsilon_{gill}\right) \quad (5a)$$

where $\delta^{41}K_{seawater}^{MRC}$ is the difference between the $\delta^{41}K$ value of the MRCs and seawater. The $\delta^{41}K$ value of MRCs can be related to the $\delta^{41}K$ value of the whole fish by combining Eq. 5a with Eq. 3

and assuming 1) that the flux of K⁺ out of MRCs *via* apical ROMK channels is small compared to the gross fluxes of K⁺ into/out of MRCs associated with K homeostasis and 2) the $\delta^{41}K$ value of plasma is similar to muscle (a reasonable assumption for most muscles in *R. norvegicus*, Figure 3B). In this case:

$$\delta^{41}K_{seawater}^{plasma/muscle} = \left(\varepsilon_{ch} - \varepsilon_{gill}\right) - \Delta f_{ch} \cdot \left(\varepsilon_{ch} - \varepsilon_{p/co}\right) \quad (6)$$

where Δf_{ch} is the relative difference in K loss *via* channels in MRCs. Although we do not independently know the value of ε_{gill} and suspect that it may vary systematically between stenohaline and euryhaline marine fish, we speculate that ~0.2–1.2‰ represents a plausible range based on results for epithelial cells in the gut of *R. norvegicus* (Figure 3B) and the maximum K isotope fractionation expected for channels (ε_{ch}). Values of ε_{ch} and $\varepsilon_{p/co}$ are assumed to be 1.2‰, and 0‰, respectively. Given these values, inspection of Eq. 6 indicates both positive and negative $\delta^{41}K_{seawater}^{plasma/muscle}$ are possible. For example, as $\Delta f_{ch} \to 0$, $\delta^{41}K_{seawater}^{plasma/muscle} \to \left(\varepsilon_{ch} - \varepsilon_{gill}\right)$ a result which yields $\delta^{41}K_{seawater}^{plasma/muscle}$ = 0 to +1‰, in agreement with measured $\delta^{41}K_{seawater}^{plasma/muscle}$ values in euryhaline marine fish. Alternatively, as $\Delta f_{ch} \to 1$, $\delta^{41}K_{seawater}^{plasma/muscle} \to \left(\varepsilon_{p/co} - \varepsilon_{gill}\right)$ a result which yields $\delta^{41}K_{seawater}^{plasma/muscle}$ = -0.2 to -1.2‰, in agreement with measured $\delta^{41}K_{seawater}^{plasma/muscle}$ values in stenohaline marine fish.

But is there any independent evidence that K homeostasis in MRCs in stenohaline marine fish operates close to a perfect "pump-leak" ($\Delta f_{ch} \sim 1$) mechanism whereas the MRCs of euryhaline marine fish operate much closer to a "leak-leak" or "pump-pump" mechanism ($\Delta f_{ch} \sim 0$)? The gill epithelium of stenohaline marine fish is considered to be more permeable than stenohaline freshwater fish due to the presence of tight-junctions connecting gill accessory cells with MRCs (Chasiotis et al., 2012). This increased permeability to NaCl must be balanced by increased NaCl secretion, a process that has been shown to be linked to the activity of NaKATP_ase in MRCs; activities of NaKATP_ase is higher in marine species than freshwater species and increase when euryhaline species are acclimated to seawater (Epstein et al., 1967; Jampol and Epstein, 1970). As an increase in the activity of NaKATP_ase activity will, all else held constant, lower f_{ch}^{in} and increase Δf_{ch}, one way of interpreting the apparent difference in Δf_{ch} between MRCs of stenohaline and euryhaline marine fish is that the more permeable gills of stenohaline marine fish require greater NaCl secretion and higher activities of NaKATPase in MRCs.

5 Conclusion

The results presented here demonstrate that K⁺ homeostasis in biological systems is associated with systematic variability in ⁴¹K/³⁹K ratios and strongly suggests

that K$^+$ transport through channels and tight-junction proteins is associated with greater fractionation of K isotopes than transport *via* pumps and co-transporters. Using results from 3 biological systems (algae, mammals, and fish) we developed a simple framework for interpreting differences in measured δ^{41}K values between intercellular fluid (ICF) and extracellular fluid (ECF) and between different internal fluid reservoirs (e.g., blood plasma and cerebrospinal fluid). If correct, this framework permits quantification of the relative importance of K$^+$ channels and pump/cotransporters in different physiological states–e.g., K depletion/excess—*in situ* (e.g., $\delta^{41}K_{plasma}^{heart}$) and in some cases *in vivo* (e.g., $\delta^{41}K_{plasma}^{urine}$). However, with the exception of *C. Reinhardtii* where the observed isotopic difference between media and the whole cell can be attributed to a single transport mechanism, our results do not directly constrain the magnitude of the individual K isotope effects associated with the machinery of K$^+$ transport. Quantifying machinery-specific K isotope effects through a combination of laboratory and numerical approaches (14) is therefore a high-priority for future research.

Data availability statement

The original contributions presented in the study are included in the article/Supplementary Material, further inquiries can be directed to the corresponding author.

Ethics statement

The animal study was reviewed and approved by USC Keck School of Medicine.

Author contributions

JH, AM, JY, DSR, and CS designed the research. JH, DSR, DH, SK, SG, and CS carried out the experiments and associated analytical measurements. JH, AM, JY, DSR, and CS interpreted the data and wrote the manuscript. All authors were involved in the revising of the manuscript.

Funding

Acknowledgments

Conflict of interest

The authors declare that the research was conducted in the absence of any commercial or financial relationships that could be construed as a potential conflict of interest.

Publisher's note

All claims expressed in this article are solely those of the authors and do not necessarily represent those of their affiliated organizations, or those of the publisher, the editors and the reviewers. Any product that may be evaluated in this article, or claim that may be made by its manufacturer, is not guaranteed or endorsed by the publisher.

Supplementary material

The Supplementary Material for this article can be found online at: https://www.frontiersin.org/articles/10.3389/fphys.2022.1016242/full#supplementary-material

References

Agarwal, R., Afzalpurkar, R., and Fordtran, J. S. (1994). Pathophysiology of potassium absorption and secretion by the human intestine. *Gastroenterology* 107, 548–571. doi:10.1016/0016-5085(94)90184-8

Barnaby, C. F., and Edmonds, C. J. (1969). Use of a miniature GM counter and a whole body counter in the study of potassium transport by the colon of normal, sodium-depleted and adrenalectomized rats *in vivo*. *J. Physiol.* 205, 647–665. doi:10.1113/jphysiol.1969.sp008988

Berneche, S., and Roux, B. (2003). A microscopic view of ion conduction through the K+ channel. *Proc. Natl. Acad. Sci. U. S. A.* 100, 8644–8648. doi:10.1073/pnas.1431750100

Betz, A. L., Firth, J. A., and Goldstein, G. W. (1980). Polarity of the blood-brain barrier: Distribution of enzymes between the luminal and antiluminal membranes of brain capillary endothelial cells. *Brain Res.* 192, 17–28. doi:10.1016/0006-8993(80)91004-5

Boron, W. F., and Boulpaep, E. L. (2005). *Medical physiology*. Philadelphia, Pennsylvania: Elsevier Saunders.

Bradbury, M., and Davson, H. (1965). The transport of potassium between blood, cerebrospinal fluid and brain. *J. Physiol.* 181, 151–174. doi:10.1113/jphysiol.1965.sp007752

Britto, D. T., and Kronzucker, H. J. (2008). Cellular mechanisms of potassium transport in plants. *Physiol. Plant.* 133, 637–650. doi:10.1111/j.1399-3054.2008.01067.x

Chasiotis, H., Kolosov, D., Bui, P., and Kelly, S. (2012). Tight junctions, tight junction proteins and paracellular permeability across the gill epithelium of fishes: A review. *Respir. Physiol. Neurobiol.* 184, 269–281. doi:10.1016/j.resp.2012.05.020

Christensen, J. N., Qin, L., Brown, S. T., and DePaolo, D. J. (2018). Potassium and calcium isotopic fractionation by plants (soybean [Glycine max], rice [Oryza sativa], and wheat [*Triticum aestivum*]). *ACS Earth Space Chem.* 2, 745–752. doi:10.1021/acsearthspacechem.8b00035

Duhm, J. (1987). Furosemide-sensitive K+ (Rb+) transport in human-erythrocytes - modes of operation, dependence on extracellular and intracellular Na+, kinetics, pH dependency, and the effect of cell-volume and N-ethylmaleimide. *J. Membr. Biol.* 98, 15–32. doi:10.1007/BF01871042

Epstein, E., Rains, D., and Elzam, O. (1963). Resolution of dual mechanisms of potassium absorption by barley roots. *Proc. Natl. Acad. Sci. U. S. A.* 49, 684–692. doi:10.1073/pnas.49.5.684

Epstein, F. H., Katz, A. I., and Pickford, G. E. (1967). Sodium- and potassium-activated adenosine triphosphatase of gills: Role in adaptation of teleosts to salt water. *Science* 156, 1245–1247. doi:10.1126/science.156.3779.1245

Evans, D. H., Piermarini, P. M., and Choe, K. P. (2005). The multifunctional fish gill: Dominant site of gas exchange, osmoregulation, acid-base regulation, and excretion of nitrogenous waste. *Physiol. Rev.* 85, 97–177. doi:10.1152/physrev.00050.2003

Foroutan, S., Brillault, J., Forbush, B., and O'Donnell, M. E. (2005). Moderate-to-severe ischemic conditions increase activity and phosphorylation of the cerebral microvascular endothelial cell Na+-K+-Cl– cotransporter. *Am. J. Physiol. Cell Physiol.* 289, C1492–C1501. doi:10.1152/ajpcell.00257.2005

Foster, E. S., Hayslett, J. P., and Binder, H. J. (1984). Mechanism of active potassium absorption and secretion in the rat colon. *Am. J. Physiol.* 246, G611–G617. doi:10.1152/ajpgi.1984.246.5.G611

Franco, R. S., Puchulu-Campanella, M. E., Barber, L. A., Palascak, M. B., Joiner, C. H., Low, P. S., et al. (2013). Changes in the properties of normal human red blood cells during *in vivo* aging. *Am. J. Hematol.* 88, 44–51. doi:10.1002/ajh.23344

Furukawa, F., Watanabe, S., Kakumura, K., Hiroi, J., and Kaneko, T. (2014). Gene expression and cellular localization of ROMKs in the gills and kidney of Mozambique tilapia acclimated to fresh water with high potassium concentration. *Am. J. Physiol. Regul. Integr. Comp. Physiol.* 307, R1303–R1312. doi:10.1152/ajpregu.00071.2014

Furukawa, F., Watanabe, S., Kimura, S., and Kaneko, T. (2012). Potassium excretion through ROMK potassium channel expressed in gill mitochondrion-rich cells of Mozambique tilapia. *Am. J. Physiol. Regul. Integr. Comp. Physiol.* 302, R568–R576. doi:10.1152/ajpregu.00628.2011

Furukawa, F., Watanabe, S., Seale, A. P., Breves, J. P., Lerner, D. T., Grau, E. G., et al. (2015). *In vivo* and *in vitro* effects of high-K+ stress on branchial expression of ROMKa in seawater-acclimated Mozambique tilapia. *Comp. Biochem. Physiol. A Mol. Integr. Physiol.* 187, 111–118. doi:10.1016/j.cbpa.2015.05.017

Garcia-Hernandez, V., Quiros, M., and Nusrat, A. (2017). Intestinal epithelial claudins: Expression and regulation in homeostasis and inflammation. *Ann. N. Y. Acad. Sci.* 1397, 66–79. doi:10.1111/nyas.13360

Gardos, G. (1958). The function of calcium in the potassium permeability of human erythrocytes. *Biochim. Biophys. Acta* 30, 653–654. doi:10.1016/0006-3002(58)90124-0

Gaymard, F., Pilot, G., Lacombe, B., Bouchez, D., Bruneau, D., Boucherez, J., et al. (1998). Identification and disruption of a plant shaker-like outward channel involved in K+ release into the xylem sap. *Cell* 94, 647–655. doi:10.1016/s0092-8674(00)81606-2

Gick, G. G., Hatala, M. A., Chon, D., and Ismail-Beigi, F. (1993). Na, K-ATPase in several tissues of the rat: Tissue-specific expression of subunit mRNAs and enzyme activity. *J. Membr. Biol.* 131, 229–236. doi:10.1007/BF02260111

Gierth, M., and Mäser, P. (2007). Potassium transporters in plants–involvement in K+ acquisition, redistribution and homeostasis. *FEBS Lett.* 581, 2348–2356. doi:10.1016/j.febslet.2007.03.035

Hibino, H., Inanobe, A., Furutani, K., Murakami, S., Findlay, I., and Kurachi, Y. (2010). Inwardly rectifying potassium channels: Their structure, function, and physiological roles. *Physiol. Rev.* 90, 291–366. doi:10.1152/physrev.00021.2009

Hickman, C. P., Jr (1968). Ingestion, intestinal absorption, and elimination of seawater and salts in the southern flounder, Paralichthys lethostigma. *Can. J. Zool.* 46, 457–466. doi:10.1139/z68-063

Hirsch, R. E., Lewis, B. D., Spalding, E. P., and Sussman, M. R. (1998). A role for the AKT1 potassium channel in plant nutrition. *Science* 280, 918–921. doi:10.1126/science.280.5365.918

Hladky, S. B., and Barrand, M. A. (2016). Fluid and ion transfer across the blood–brain and blood–cerebrospinal fluid barriers; a comparative account of mechanisms and roles. *Fluids Barriers CNS* 13, 19–69. doi:10.1186/s12987-016-0040-3

Hofmann, A. E., Bourg, I. C., and DePaolo, D. J. (2012). Ion desolvation as a mechanism for kinetic isotope fractionation in aqueous systems. *Proc. Natl. Acad. Sci. U. S. A.* 109, 18689–18694. doi:10.1073/pnas.1208184109

Jampol, L. M., and Epstein, F. H. (1970). Sodium-potassium-activated adenosine triphosphatase and osmotic regulation by fishes. *Am. J. Physiol.* 218, 607–611. doi:10.1152/ajplegacy.1970.218.2.607

Jones, A. W., Sander, P. D., and Kampschmidt, D. L. (1977). The effect of norepinephrine on aortic 42K turnover during deoxycorticosterone acetate hypertension and antihypertensive therapy in the rat. *Circ. Res.* 41, 256–260. doi:10.1161/01.res.41.2.256

Katzman, R., Graziani, L., Kaplan, R., and Escriva, A. (1965). Exchange of cerebrospinal fluid potassium with blood and brain: Study in normal and ouabain perfused cats. *Arch. Neurol.* 13, 513–524. doi:10.1001/archneur.1965.00470050061007

Kochian, L. V., and Lucas, W. J. (1982). Potassium transport in corn roots: I. Resolution of kinetics into a saturable and linear component. *Plant Physiol.* 70, 1723–1731. doi:10.1104/pp.70.6.1723

Kolosov, D., Bui, P., Chasiotis, H., and Kelly, S. P. (2013). Claudins in teleost fishes. *Tissue barriers.* 1, e25391. doi:10.4161/tisb.25391

Kopec, W., Köpfer, D. A., Vickery, O. N., Bondarenko, A. S., Jansen, T. L., De Groot, B. L., et al. (2018). Direct knock-on of desolvated ions governs strict ion selectivity in K+ channels. *Nat. Chem.* 10, 813–820. doi:10.1038/s41557-018-0105-9

Lacombe, B., Pilot, G., Michard, E., Gaymard, F., Sentenac, H., and Thibaud, J.-B. (2000). A shaker-like K+ channel with weak rectification is expressed in both source and sink phloem tissues of Arabidopsis. *Plant Cell* 12, 837–851. doi:10.1105/tpc.12.6.837

Lebaudy, A., Véry, A.-A., and Sentenac, H. (2007). K+ channel activity in plants: Genes, regulations and functions. *FEBS Lett.* 581, 2357–2366. doi:10.1016/j.febslet.2007.03.058

Li, W., Kwon, K. D., Li, S., and Beard, B. L. (2017). Potassium isotope fractionation between K-salts and saturated aqueous solutions at room temperature: Laboratory experiments and theoretical calculations. *Geochimica Cosmochimica Acta* 214, 1–13. doi:10.1016/j.gca.2017.07.037

MacKinnon, R. (2003). Potassium channels. *FEBS Lett.* 555, 62–65. doi:10.1016/s0014-5793(03)01104-9

Maetz, J. (1969). Seawater teleosts: Evidence for a sodium-potassium exchange in the branchial sodium-excreting pump *Science* 166, 613–615. doi:10.1126/science.166.3905.613

Malhotra, B., and Glass, A. D. (1995). Potassium fluxes in Chlamydomonas reinhardtii (I. Kinetics and electrical potentials). *Plant Physiol.* 108, 1527–1536. doi:10.1104/pp.108.4.1527

Marchand, J., Heydarizadeh, P., Schoefs, B., and Spetea, C. (2020). "Chloroplast ion and metabolite transport in algae," in *Photosynthesis in algae: Biochemical and physiological mechanisms*. Editors A. W. D. Larkum, A. R. Grossman, and J. A. Raven (Cham: Springer International Publishing), 107–139.

McDonough, A. A., and Youn, J. H. (2017). Potassium homeostasis: The knowns, the unknowns, and the health benefits. *Physiol. (Bethesda)* 32, 100–111. doi:10.1152/physiol.00022.2016

Mironenko, A., Zachariae, U., de Groot, B. L., and Kopec, W. (2021). The persistent question of potassium channel permeation mechanisms. *J. Mol. Biol.* 433, 167002. doi:10.1016/j.jmb.2021.167002

Morgan, L. E., Ramos, D. P. S., Davidheiser-Kroll, B., Faithfull, J., Lloyd, N. S., Ellam, R. M., et al. (2018). High-precision $^{41}K/^{39}K$ measurements by MC-ICP-MS indicate terrestrial variability of $\delta^{41}K$. *J. Anal. At. Spectrom.* 33, 175–186. doi:10.1039/c7ja00257b

Mulkidjanian, A. Y., Bychkov, A. Y., Dibrova, D. V., Galperin, M. Y., and Koonin, E. V. (2012). Origin of first cells at terrestrial, anoxic geothermal fields. *Proc. Natl. Acad. Sci. U. S. A.* 109, E821–E830. doi:10.1073/pnas.1117774109

Noble, E. E., Hahn, J. D., Konanur, V. R., Hsu, T. M., Page, S. J., Cortella, A. M., et al. (2018). Control of feeding behavior by cerebral ventricular volume transmission of melanin-concentrating hormone. *Cell Metab.* 28, 55–68. doi:10.1016/j.cmet.2018.05.001

Pilot, G., Lacombe, B. t., Gaymard, F., Chérel, I., Boucherez, J., Thibaud, J.-B., et al. (2001). Guard cell inward K+ channel activity inarabidopsis involves expression of the twin channel subunits KAT1 and KAT2. *J. Biol. Chem.* 276, 3215–3221. doi:10.1074/jbc.M007303200

Ramos, D. P. S., Coogan, L. A., Murphy, J. G., and Higgins, J. A. (2020). Low-temperature oceanic crust alteration and the isotopic budgets of potassium and

magnesium in seawater. *Earth Planet. Sci. Lett.* 541, 116290. doi:10.1016/j.epsl.2020.116290

Ramos, D. P. S., Morgan, L. E., Lloyd, N. S., and Higgins, J. A. (2018). Reverse weathering in marine sediments and the geochemical cycle of potassium in seawater: Insights from the K isotopic composition (K-41/K-39) of deep-sea pore-fluids. *Geochimica Cosmochimica Acta* 236, 99–120. doi:10.1016/j.gca.2018.02.035

Rolfe, D. F., and Brown, G. C. (1997). Cellular energy utilization and molecular origin of standard metabolic rate in mammals. *Physiol. Rev.* 77, 731–758. doi:10.1152/physrev.1997.77.3.731

Roux, B. (2017). Ion channels and ion selectivity. *Essays Biochem.* 61, 201–209. doi:10.1042/EBC20160074

Rui, H., Artigas, P., and Roux, B. (2016). The selectivity of the Na+/K+-pump is controlled by binding site protonation and self-correcting occlusion. *Elife* 5, e16616. doi:10.7554/eLife.16616

Sachs, J. R. (1971). Ouabain-insensitive sodium movements in the human red blood cell *J. Gen. Physiol.* 57, 259–282. doi:10.1085/jgp.57.3.259

Stautz, J., Hellmich, Y., Fuss, M. F., Silberberg, J. M., Devlin, J. R., Stockbridge, R. B., et al. (2021). Molecular mechanisms for bacterial potassium homeostasis. *J. Mol. Biol.* 433, 166968. doi:10.1016/j.jmb.2021.166968

Terner, C., Eggleston, L., and Krebs, H. (1950). The role of glutamic acid in the transport of potassium in brain and retina. *Biochem. J.* 47, 139–149. doi:10.1042/bj0470139

Tosteson, D. C., and Hoffman, J. F. (1960). Regulation of cell volume by active cation transport in high and low potassium sheep red cells. *J. Gen. Physiol.* 44, 169–194. doi:10.1085/jgp.44.1.169

Tsai, P.-Y., Zhang, B., He, W.-Q., Zha, J.-M., Odenwald, M. A., Singh, G., et al. (2017). IL-22 upregulates epithelial claudin-2 to drive diarrhea and enteric pathogen clearance. *Cell Host Microbe* 21, 671–681. e674. doi:10.1016/j.chom.2017.05.009

Van Renterghem, C., Vigne, P., and Frelin, C. (1995). A charybdotoxin-sensitive, Ca2+-activated K+ channel with inward rectifying properties in brain microvascular endothelial cells: Properties and activation by endothelins. *J. Neurochem.* 65, 1274–1281. doi:10.1046/j.1471-4159.1995.65031274.x

Wang, K., and Jacobsen, S. B. (2016). An estimate of the Bulk Silicate Earth potassium isotopic composition based on MC-ICPMS measurements of basalts. *Geochimica Cosmochimica Acta* 178, 223–232. doi:10.1016/j.gca.2015.12.039

Youn, J. H., and McDonough, A. A. (2009). Recent advances in understanding integrative control of potassium homeostasis. *Annu. Rev. Physiol.* 71, 381–401. doi:10.1146/annurev.physiol.010908.163241

Yu, H., Noskov, S. Y., and Roux, B. (2010). Two mechanisms of ion selectivity in protein binding sites. *Proc. Natl. Acad. Sci. U. S. A.* 107, 20329–20334. doi:10.1073/pnas.1007150107

Zeng, H., Rozsa, V. F., Nie, N. X., Zhang, Z., Pham, T. A., Galli, G., et al. (2019). *Ab initio* calculation of equilibrium isotopic fractionations of potassium and rubidium in minerals and water. *ACS Earth Space Chem.* 3, 2601–2612. doi:10.1021/acsearthspacechem.9b00180